Received: 15 January 2025 | Revised: 8 June 2025 | Accepted: 24 July 2025

DOI: 10.1002/aic.70023

AIChE JOURNAL

RESEARCH ARTICLE

Separations: Materials, Devices and Processes

Carbanion engineering for highly efficient selective SO_2 capture by ionic liquids based commercializable polymers

Guokai Cui[1] | Yinfeng Chen[1] | Limin Xu[1] | Ruina Zhang[1] | Xu Wang[1] | Ying Zhou[1] | Quanli Ke[1] | Xiaopo Niu[1] | Xiangping Zhang[2] | Mingcai Teng[3] | Meichao Li[1] | Hanfeng Lu[1]

[1]Innovation Team of Air Pollution Control, Institute of Catalytic Reaction Engineering, Zhejiang Key Laboratory of Surface and Interface Science and Engineering for Catalysts, State Key Laboratory of Green Chemical Synthesis and Conversion, College of Chemical Engineering, Zhejiang University of Technology, Hangzhou, China

[2]Beijing Key Laboratory of Ionic Liquids Clean Process, CAS Key Laboratory of Green Process and Engineering, State Key Laboratory of Multiphase Complex Systems, Institute of Process Engineering, Chinese Academy of Sciences, Beijing, China

[3]Zhejiang Changhong Biological Material Co., Ltd., Shaoxing, China

Correspondence
Guokai Cui and Hanfeng Lu, Innovation Team of Air Pollution Control, Institute of Catalytic Reaction Engineering, Zhejiang Key Laboratory of Surface and Interface Science and Engineering for Catalysts, State Key Laboratory of Green Chemical Synthesis and Conversion, College of Chemical Engineering, Zhejiang University of Technology, Hangzhou 310014, China.
Email: chemcgk@163.com; luhf@zjut.edu.cn

Funding information
Key Research and Development Projects in Zhejiang Province, Grant/Award Numbers: 2024C03108, 2023C03127, 2024C03114, 2024C03121; National Natural Science Foundation of China, Grant/Award Numbers: 22378353, 22208300; Zhejiang Provincial Natural Science Foundation of China, Grant/Award Number: LTGS24E080008; Zhejiang Provincial Postdoctoral Science Foundation, Grant/Award Number: ZJ2023145

Abstract

Development of alternative ionic liquid-based porous materials functionalized with active sites for highly efficient selective and reversible SO_2 capture is highly desired. Here, conjugated carbanion ILs based commercializable $[N_{1111}][TTFA]$@polymer and $[N_{1111}][BTFA]$@polymer exhibited macroreticular internal structures and macropores (>50 nm) as well as enhanced hydrophobicity. Efficient SO_2 capture (>7 mmol g^{-1}), high SO_2/CO_2 and SO_2/H_2O selectivity could be obtained. Adsorption isotherms were correlated using Langmuir, Freundlich, and Sips models. The results of adsorption experiments, FT-IR spectroscopy, and quantum chemical calculations suggested that the $SO_2\cdots$IL@polymer charge-transfer quasi-chemical interaction is the key role for highly efficient selective SO_2 capture. Initial isosteric heat (10–20 kJ mol^{-1}) increased with SO_2 loading. To our best knowledge, this is the first example of using conjugated carbanion-derived IL-based commercializable polymers for highly efficient selective SO_2 capture. The carbanion engineering strategy opens a door to obtain enhanced hydrophobicity as well as efficient selective SO_2 capture by IL-based commercializable polymers.

KEYWORDS
carbanion, commercializable polymer, ionic liquid, separation, SO_2 adsorption

1 | INTRODUCTION

Sulfur compounds are existing in the fossil fuels, and transform to sulfur dioxide (SO_2) in flue gas via burning. It is known that flue gas usually contains CO_2, SO_2, water vapor, etc., and SO_2 in atmosphere threatens the environment and human health. Conventional limestone scrubbing, ammonia scrubbing, and organic solvents absorption result in low-quality byproducts and waste water.[1] Therefore, new efficient and economical SO_2 sorbent materials must be developed for selective capture, aligning with resource sustainability and environmental protection.[2]

Ionic liquids (ILs), composed of organic/inorganic anions and organic cations, are organic liquids at room temperature or below 100°C at least. In recent decades, ILs have been applied for efficient

capture and separation of gases such as CO_2,[3–10] SO_2,[11–14] H_2S,[15–18] NO_x,[19–22] NH_3,[23–27] CO,[28–30] etc., because of their tunable structures and unique properties, including non-flammability, low vapor pressure, and high thermal–chemical stability.[31–33] For SO_2 capture, Han et al.[34] reported that SO_2 capture by functionalized guanidinium IL and a capacity of 0.978 mol/mol SO_2 could be achieved at 40°C under 8% SO_2 in N_2. Another typical example reported by Wang et al.[35] is that about IL:SO_2 = 1:2 chemisorption capacity could be reached through multiple site interaction by azolate-functionalized ILs under 0.1 bar SO_2. There has been a rapid development of the design and synthesis of ILs for SO_2 capture during this decade.[12,36] It is reported that most ILs with kinds of functional groups could reach about 1 and 0.1 g g^{-1} SO_2 capacities at room temperature and 1 or 0.1 bar SO_2, respectively. However, high capacity indicates strong interaction energy or high sorption enthalpy. Besides, the viscosity increased during SO_2 chemisorption, which limits the gas diffusion rate.[37] Thus, the development of alternative sorbents is necessary for SO_2 capture. Recently, ionic porous organic materials (iPOMs) have been applied for SO_2 capture with increased capacity due to the active sites and pore structures. These iPOMs include poly(ionic liquid)s (PILs),[38] ionic metal–organic frameworks (MOFs),[39] ionic metal–organic cages (MOCs),[40] ionic covalent organic frameworks (COFs),[41] ionic covalent triazine frameworks (CTFs),[42] and ionic hyper-crosslinked polymers (HCPs),[43,44] etc. Although MOFs, MOCs, COFs, CTFs, and HCPs seem to be the most promising because of their tunable topology and pore size, the expensive ligands as well as tedious preparation processes with low yields make them difficult to apply in industry. Commercial Amberlite®IRA-900 is a kind of cation-crosslinked macro-porous PILs.[45] Additionally, it is known that this kind of polymer is more hydrophilic.[46] Thus, the anion could be functionalized, and polymers could be applied for highly efficient selective and reversible capture of SO_2.

Herein, we prepared a series of conjugated carbanion functionalized IL-based commercializable polymers, including [N_{1111}][TTFA]@polymer with thenoyltrifluoroacetonate anion and [N_{1111}][BTFA]@polymer with benzoyltrifluoroacetonate anion for SO_2 capture and SO_2/CO_2 separation. [N_{1111}][Br]@polymer with bromide anion was also prepared for comparison (Figure 1). These polymers exhibited the macroreticular internal structures and the macropores (>50 nm). The effect of SO_2 partial pressure and temperature on SO_2 adsorption capacity resulted in the efficient SO_2 capture (>7 mmol g^{-1}) and the high SO_2/CO_2 selectivity (62.6-fold) and SO_2/H_2O selectivity (0.36-fold) in the ratio of mmol g^{-1} by the conjugated carbanion. The adsorption isotherms were correlated using Langmuir, Freundlich, and Sips models. FT-IR spectroscopy and quantum chemical calculations were used to investigate the $SO_2\cdots$IL@polymer interactions. The carbanion

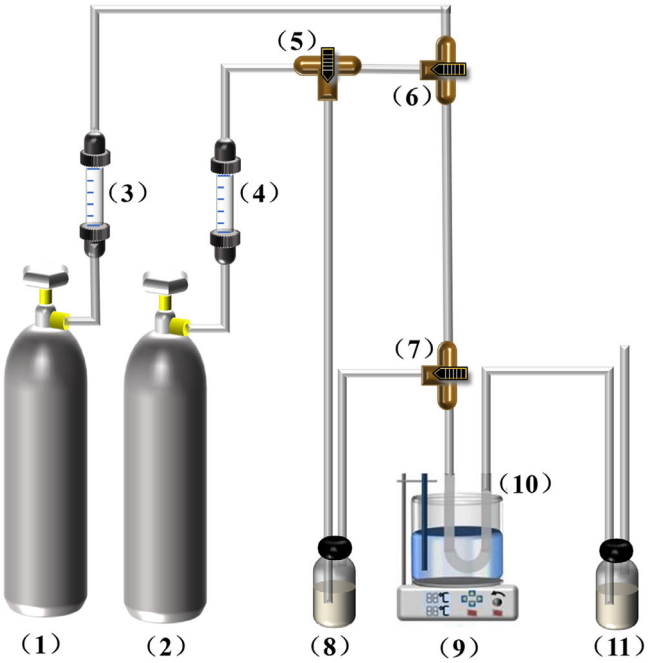

FIGURE 2 Schematic diagram of gas absorption experimental device diagram. (1) SO_2 gas cylinder; (2) N_2 gas cylinder; (3,4) flow meter; (5–7) three-way valve; (8) flask with water in it; (9) water bath; (10) U-shaped tube; (11) exhaust gas treatment (NaOH aqueous solution).

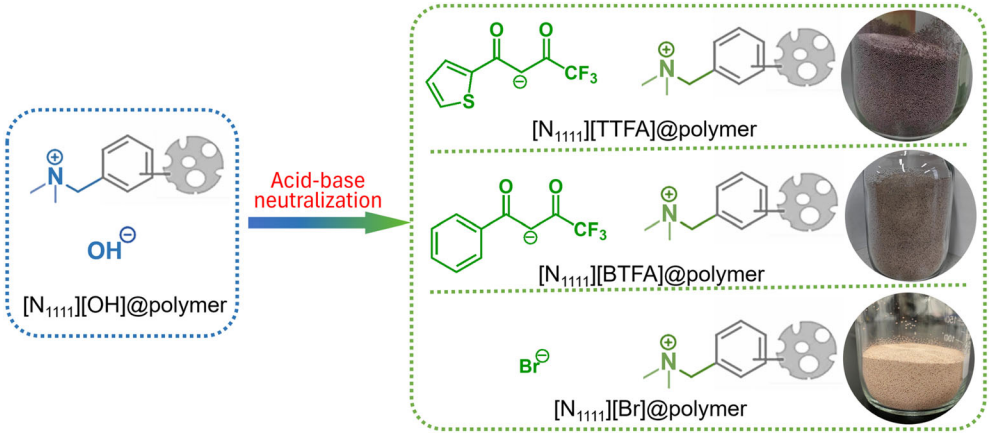

FIGURE 1 Synthesis and structures of functional IL@polymers.

engineering strategy designing conjugated carbanion functional adsorbents opens a door to obtain enhanced hydrophobicity as well as efficient selective SO_2 capture by IL-based commercializable iPOMs.

2 | EXPERIMENTAL METHODS

2.1 | Materials

Amberlite® IRA-900(OH) ([N_{1111}][OH]@polymer, CAS No. 9017-79-2) was approached from Sinopharm Chemical Reagent Co., Ltd. Thenoyltrifluoroacetone (TTFA, 98%, CAS No. 206-316-7) and 3-benzoyl 1,1,1-trifluoroacetate (BTFA, 97%, CAS No. 326-06-7) were bought from Shanghai Bide Pharmaceutical Technology Co., Ltd. Hydrobromic acid (HBr, 40%, CAS No. 10035-10-6) was approached from Sinopharm Chemical Reagent Co., Ltd. SO_2 (99.99%), CO_2 (99.995%) and N_2 (99.99%) were supplied from Hangzhou Jingong Gas Co., Ltd.

2.2 | Synthesis of IL@polymers

These IL@polymers could be easily prepared from [N_{1111}][OH]@polymer and different proton donors (TTFA, BTFA, and HBr) by acid–base neutralization. Take the preparation of [N_{1111}][TTFA]@polymer as an example. Briefly, [N_{1111}][OH]@polymer was first activated by an ethanol solution of NaOH and then transferred to the ion exchange column and washed with ethanol to remove excess NaOH. Afterwards, excess ethanol solution of TTFA was added to the ion exchange column for the acid–base neutralization reaction with [N_{1111}][OH]@polymer. When the reaction was finished, the polymer was washed with ethanol to remove excess TTFA, and [N_{1111}][TTFA]@polymer could be obtained readily after

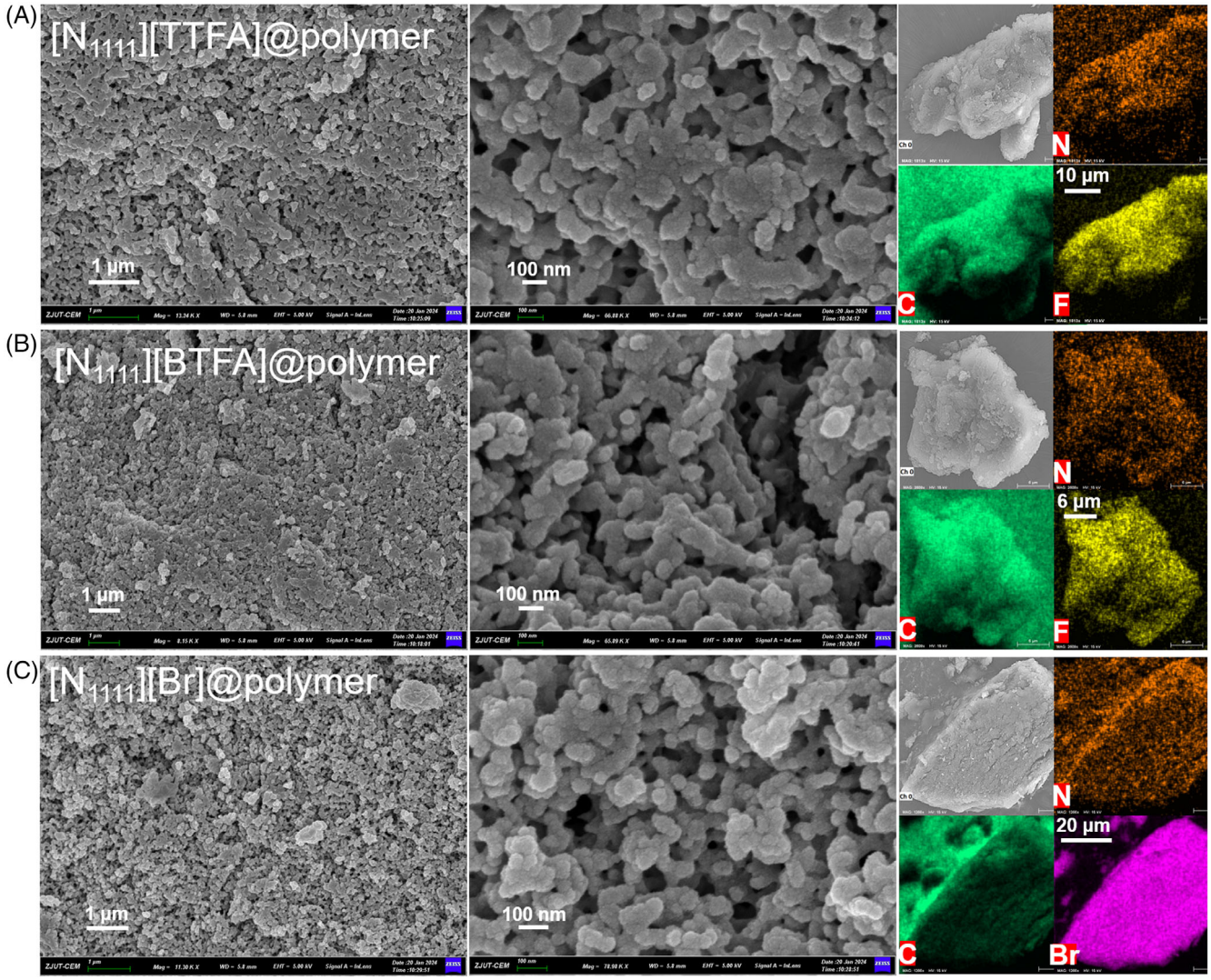

FIGURE 3 SEM images and EDS mapping images of [N_{1111}][TTFA]@polymer (A), [N_{1111}][BTFA]@polymer (B), and [N_{1111}][Br]@polymer (C).

evaporation and drying under vacuum at 60°C for 24 h to remove ethanol and water.

2.3 | Synthesis of conjugated carbanion functionalized ILs

For the synthesis of $[N_{1111}][TTFA]$, equimolar TTFA and anhydrous LiOH were stirred in 50 mL ethanol solution at 40°C for 6 h, then evaporated at 80°C and dried in vacuum at 80°C to obtain [Li][TTFA]. Subsequently, the equimolar [Li][TTFA] and $[N_{1111}][Br]$ were mixed in CH_2Cl_2/H_2O solvent (4:1 in v/v) and stirred at room temperature for 4 h. The organic phase was extracted twice with deionized water, and evaporated at 50°C to remove CH_2Cl_2, and then dried in vacuum at 60°C for 4 h to obtain $[N_{1111}][TTFA]$. $[N_{1111}][BTFA]$ was obtained by the same method.

2.4 | Characterization

The morphology of samples was examined by the field emission scanning electron microscopy (SEM, Sigma 360). Surface functional moieties were tested using X-ray photoelectron spectroscopy (XPS, Thermo Scientific K-Alpha). The elemental analysis was conducted using an elemental analyzer (Elementar UNICUBE). N_2 adsorption–desorption isotherms and specific surface areas were recorded at 77 K using the Micromeritics 3Flex, with the Barret–Joyner–Halenda (BJH) model. Thermogravimetric analysis (TGA) was performed on a Netzsch TG209F3 Tarsus instrument from room temperature to 800°C in an N_2 atmosphere at a rate of 10°C min^{-1}. The water contact angles were measured on an automatic video contact angle tester (Chengde Dingsheng JY-82C, China), using the sessile drop method. Fourier transform

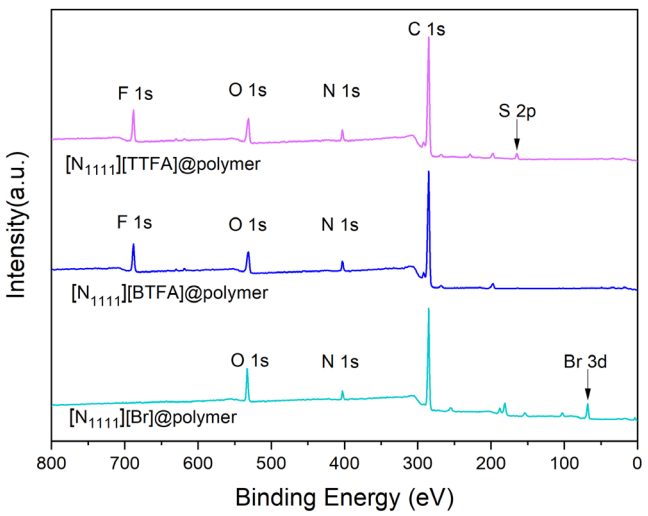

FIGURE 4 Full survey XPS spectra of $[N_{1111}][TTFA]$@polymer, $[N_{1111}][BTFA]$@polymer, and $[N_{1111}][Br]$@polymer.

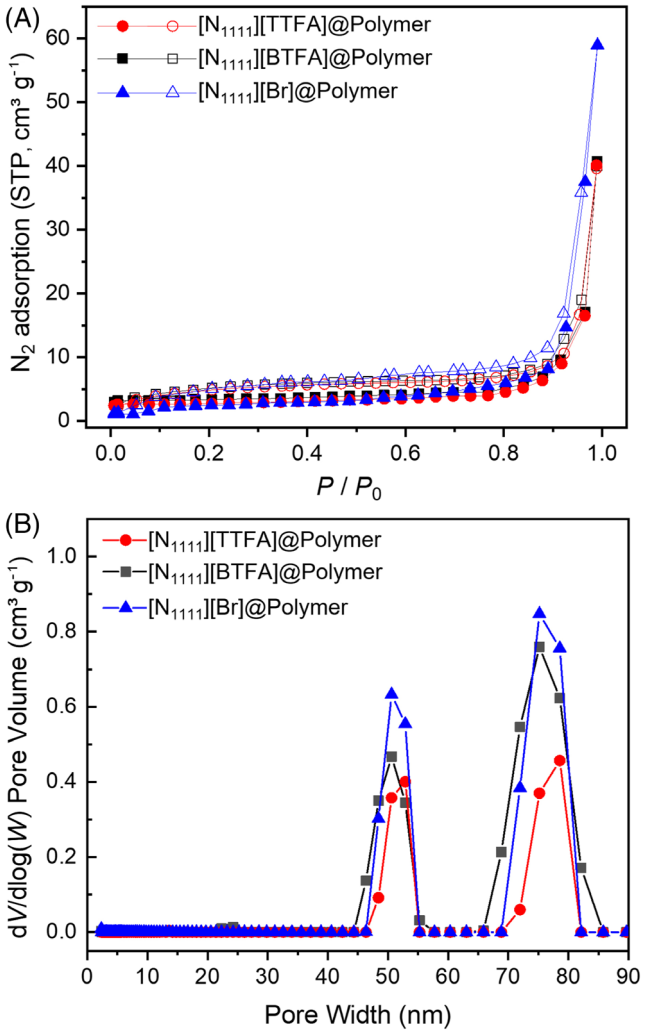

FIGURE 5 N_2 adsorption–desorption isotherms (A) and pore sizes (B) of $[N_{1111}][TTFA]$@polymer, $[N_{1111}][BTFA]$@polymer, and $[N_{1111}][Br]$@polymer.

TABLE 1 BET surface area (S_{BET}, in $m^2\ g^{-1}$), total pore volume (V_{tot}, in $cm^3\ g^{-1}$), average pore size (D_{av}, in nm), element analysis of N content (N, in wt%), IL-moieties content (C_{IL}, in mmol g^{-1}) based on N wt%, onset decomposition temperature (T_{onset}, in°C), contact angle (θ, in°), SO_2 adsorption at 20°C and 1 bar (Z_{SO_2}, in mmol g^{-1}), isosteric heat of SO_2 adsorption (Q_{st}, in kJ mol^{-1}), and CO_2 adsorption at 20°C and 1 bar (Z_{SO_2}, in mmol g^{-1}) of IL@polymers in this work.

Polymer	S_{BET}	V_{tot}	D_{av}	N	C_{IL}	T_{onset}	θ	Z_{SO_2}	Q_{st}	Z_{CO_2}
$[N_{1111}][TTFA]$@polymer	19.36	0.21	63	3.35	2.393	209.7	73.84	7.51	12.7	0.12
$[N_{1111}][BTFA]$@polymer	19.73	0.22	62	3.47	2.479	211.5	62.96	7.09	17.9	0.15
$[N_{1111}][Br]$@polymer	23.48	0.25	65	3.41	2.436	210.1	24.10	7.53	17.5	0.34

infrared (FT-IR) spectra were measured on a Thermo Scientific Nicolet iS 20 IR spectrometer in the region of 4000–400 cm^{-1}.

2.5 | Gas adsorption

The SO_2 adsorption and desorption were measured according to the literature,[47] and the schematic diagram of the process was illustrated in Figure 2. SO_2 adsorptions on IL@polymers were performed according to the following dynamic method under different partial pressures and temperatures; the mass of samples was measured on an electronic balance with an accuracy of ±0.0001 g. IL@polymer with known mass, m_1 in grams, was added into the U-shaped tube with an inner diameter of 7 mm. The tube was immersed in a water bath with desired temperatures. Then, SO_2 with different concentrations was introduced into the tube with a flow rate of 60 mL min^{-1} through stainless steel pipelines. Aqueous NaOH solution was used to absorb SO_2 and purify the exhaust gas. The mass of SO_2-adsorbed IL@polymer, m_2 in gram, was measured during adsorption until it no longer changed, indicating that the equilibrium was obtained. The adsorption capacity (Z, in mmol g^{-1}) can be calculated by:

$$Z = \frac{(m_2 - m_1) \div 64}{m_1} \times 1000$$

Desorptions of SO_2 were performed at 80°C under 100% N_2 at 1 bar. The uncertainty of mass was measured to be ±0.07.

The water adsorptions on IL@polymers were performed according to the similar dynamic method as SO_2 adsorption. Briefly, 100 vol % N_2 with a flow rate of 100 mL min^{-1} was bubbling through the deionized water and introduced into the tube, containing IL@polymer with known mass, through stainless steel pipelines. The mass of H_2O-adsorbed IL@polymer was measured during adsorption until it no longer changed, indicating that the equilibrium was obtained. The CO_2 adsorptions on IL@polymers were performed on Micromeritics 3Flex using the volumetric method.

3 | RESULTS AND DISCUSSION

3.1 | Structural characterization of IL@polymers

All three polymers $[N_{1111}][TTFA]$@polymer, $[N_{1111}][BTFA]$@polymer, and $[N_{1111}][Br]$@polymer were synthesized via acid–base neutralization with corresponding acids from the raw material $[N_{1111}][OH]$@polymer. The surface morphology of well-synthesized IL@polymer adsorbents was characterized by SEM (Figure 3). It can be seen that the macroreticular internal structures and the macropores (>50 nm), originating from "glueing" of polymer nodules.[48] The SEM images also show that a large number of mesoporous–macroporous structures are uniformly distributed on the surface of the materials, and these porous structures are conducive to the exposure of more adsorption sites and provide a micro-reactive environment for SO_2 capture. The results of energy dispersive spectroscopy (EDS) elemental mapping suggested the successful synthesis of $[N_{1111}][TTFA]$@polymer, $[N_{1111}][BTFA]$@polymer, and $[N_{1111}][Br]$@polymer. Besides, in the XPS survey spectra, the characteristic peaks of Br 3d, S 2p, C 1s, N 1s, O 1s, and F 1s are located at 68.1, 164.9, 285.2, 402.8, 531.8, and 688.1 eV, respectively, also suggesting that the three modified polymers were successfully synthesized (Figure 4). According to the content of N in IRA-900 via elemental analysis, the contents of IL-moieties in these IL@polymers were around 2.4 mmol g^{-1} (Table 1).

According to the IUPAC classification, the N_2 adsorption–desorption isotherms show a type III shape (Figure 5),[49] and the BET surface area (S_{BET}, in m^2 g^{-1}), the total pore volume (V_{tot}, in cm^3 g^{-1}), as well as the average pore size (D_{av}, in nm) were collected in Table 1. It can be seen that the adsorbate uptake increases exponentially with increasing pressure, and the increase continues until the relative pressure reaches unity, resulting in the

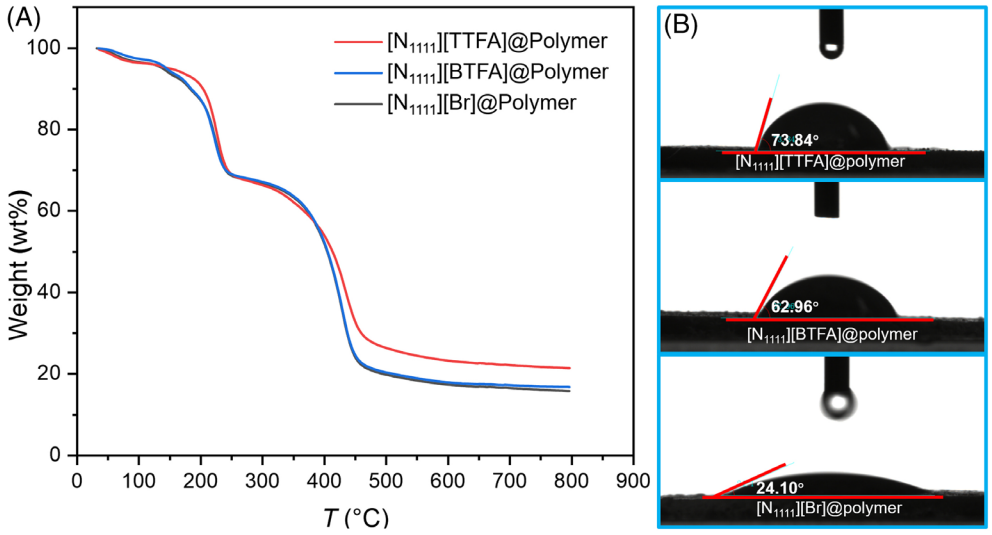

FIGURE 6
Thermogravimetric analysis curves (A) and water contact angles (B) of $[N_{1111}][TTFA]$@polymer, $[N_{1111}][BTFA]$@polymer, and $[N_{1111}][Br]$@polymer.

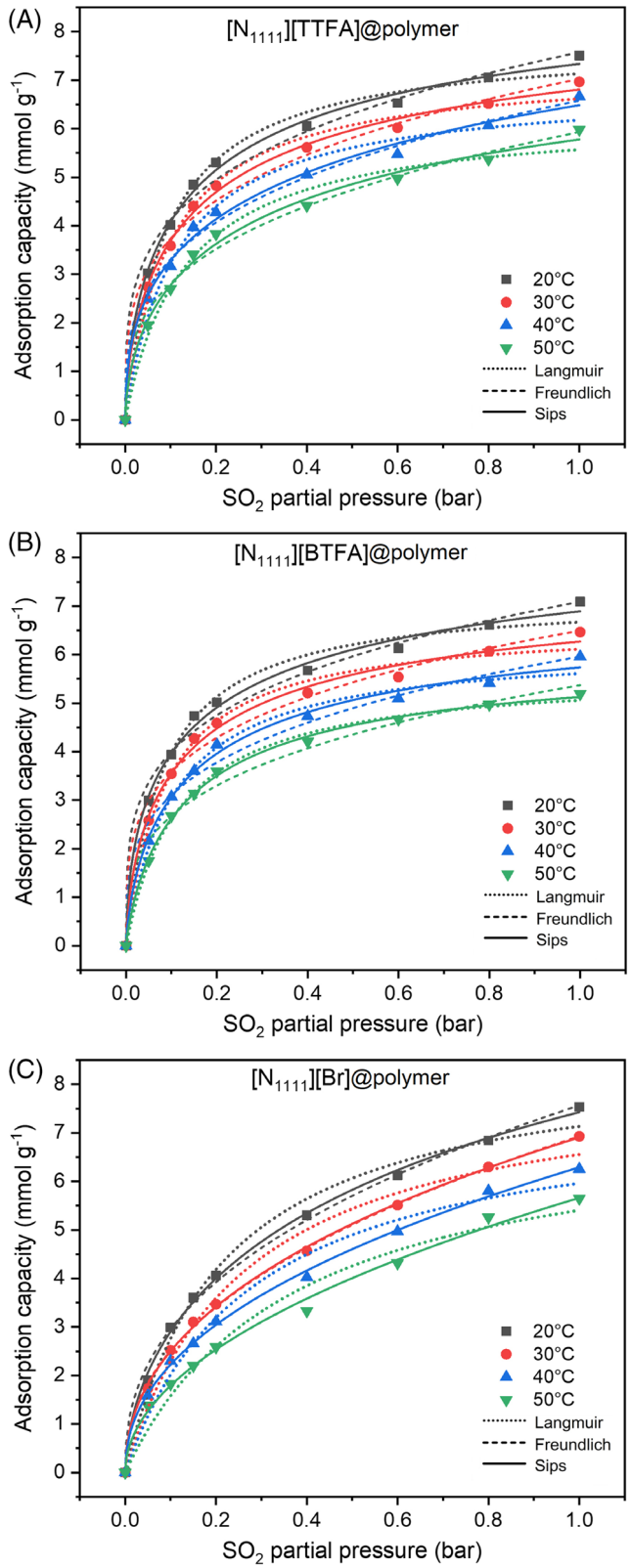

FIGURE 7 SO_2 adsorption isotherms of $[N_{1111}][TTFA]$@polymer (A), $[N_{1111}][BTFA]$@polymer (B), and $[N_{1111}][Br]$@polymer (C).

adsorbate–adsorbate interaction being big compared to the adsorbate–sorbent interaction.[50,51] The obtained specific surface areas of $[N_{1111}][TTFA]$@polymer, $[N_{1111}][BTFA]$@polymer, and $[N_{1111}][Br]$@polymer are measured to be 19.36, 19.73, and 23.48 $m^2\ g^{-1}$, respectively, while the average pore sizes for these polymers were measured to be 63, 62, and 65 nm, suggesting the limited surface areas and macropore sizes of these IL@polymer adsorbents. From [Br]-based IL@polymer to conjugated carbanion-derived IL@polymers, the BET surface area, the total pore volume, and the average pore size were all slightly decreased with the increase of anion size.

TABLE 2 Comparison of SO_2 capacities of typical SO_2-philic ILs and PILs.

Sorbent	T (°C)	SO_2 capacity (mmol g^{-1}) 1 bar	0.1 bar	Ref.
$[N_{1111}][TTFA]$@polymer	20	7.51	4.02	This work
$[N_{1111}][BTFA]$@polymer	20	7.09	3.94	This work
$[N_{1111}][Br]$@polymer	20	7.53	2.99	This work
$[N_{1111}][OH]$@polymer	20	10.39	1.65	This work
$[P_{66614}][Im]$	20	8.75	3.75	35
$[P_{66614}][4\text{-Br-PhCOO}]$	20	6.03	2.43	54
$[P_{66614}][4\text{-CN-PhCOO}]$	20	6.20	1.73	55
$[P_{66614}][4\text{-CHO-PhCOO}]$	20	5.69	2.52	56
[K(TX-7)][SCN]	20	6.32	1.61	57
$[P_{66614}][SCN]$	20	5.94	2.03	58
$[E_1mim][MeSO_3]$	30	9.73	–	59
$[Et_2NEmim][PF_6]$	30	6.41	2.81	60
$[Et_2NEmim][Tf_2N]$	20	6.07	1.92	61
$[P_{66614}][Phth]$	20	7.03	0.72	62
$[P_{4442}][PySO_3]$	20	9.47	1.51	63
$[Li(TDA\text{-}1)][Tf_2N]$	20	7.40	2.15	64
[Na(PEG-400)][Tetz]	30	6.86	2.78	65
P([TMG][A])	25	4.06	–	66
P([TMG][A]-co-MBA)	20	4.69	–	67
HNIP-DCX-1	25	4.80	1.56	68
$[MFM\text{-}305\text{-}CH_3][Cl]$	25	5.16	–	69
ICTF-[Cl]	25	6.5	–	42
P([allyl-HMTA][Br]-DVB)	25	6.10	0.99	70
$P(D[VImC_6][Br])$	25	7.78	1.56	38
TBM-Bentriz	25	5.83	2.98	71
P(EVIm-Br)	25	10.51	3.29	72

TGA, measuring the mass change of a sample as a function of temperature or time, could be used to test the thermal stability of IL@polymers. It can be seen from Figure 6A that the trends of all three weight loss curves are similar, and the degradation behavior including three stages separated by 100 and 250°C are the evaporation of water, the degradation of ammonium IL-moieties, and the degradation of polymer backbones.[46] Overall, the TGA results indicate that the three IL@polymers have excellent thermal stability and can be heated to satisfy the desorption of SO_2 by heating the adsorbent, further supporting their potential for reversible SO_2 adsorption. The

results showed that the onset decomposition temperatures (T_{onset}) were measured to be 209.7, 211.5, and 210.1°C for $[N_{1111}][TTFA]$@polymer, $[N_{1111}][BTFA]$@polymer, and $[N_{1111}][Br]$@polymer, respectively, indicating high thermostability. To determine the hydrophobicity property, the water contact angles for $[N_{1111}][TTFA]$@polymer, $[N_{1111}][BTFA]$@polymer, and $[N_{1111}][Br]$@polymer were measured to be 73.84°, 62.96°, and 24.10°, respectively, indicating the conjugated carbanion-derived IL@polymers are more hydrophobic than bromide-based IL@polymer (Figure 6B).[52] The solubilities of ILs $[N_{1111}][TTFA]$, $[N_{1111}][BTFA]$, and $[N_{1111}][Br]$ were also tested to verify the hydrophobicity property of these IL@polymers. The solubilities of $[N_{1111}][TTFA]$ and $[N_{1111}][BTFA]$ were measured to be 0.61 and 0.81 g IL per 100 g H_2O, respectively, while that of $[N_{1111}][Br]$ was measured to be 31.84 g IL per 100 g H_2O, suggesting that conjugated carbanion-derived IL@polymers are more hydrophobic than [Br]-based IL@polymer.

3.2 | SO_2 adsorption isotherms

SO_2 capture at different temperatures and partial pressures by these IL@polymers was measured, and the SO_2 adsorption isotherms of IL@polymers are illustrated in Figure 7, suggesting the similar trends of SO_2 adsorption performances by these IL@polymers. SO_2 adsorption capacities decreased with the decrease of SO_2 partial pressure. For SO_2 adsorption on conjugated carbanion-derived IL@polymers, the SO_2 absorption capacity of $[N_{1111}][TTFA]$@polymer at 20°C decreased from 7.51 mmol g^{-1} under 1 bar to 3.02 mmol g^{-1} under 0.05 bar, indicating that captured SO_2 could be desorbed under low partial pressure. While for SO_2 adsorption on $[N_{1111}][Br]$@polymer, the SO_2 absorption capacity at 20°C decreased from 7.53 mmol g^{-1} under 1 bar to 1.91 mmol g^{-1} under 0.05 bar. The results suggested that IL@polymers with conjugated carbanions exhibited more efficient SO_2 adsorption under low partial pressure. The comparison of the SO_2 capture performance with other typical ILs and PILs can be found in Table 2, which indicated that the conjugated carbanion-derived IL@polymers could efficiently capture SO_2, especially under low partial pressure. The effect of adsorption temperature on SO_2 capture capacity of these IL@polymers was also investigated. The results showed that the SO_2 adsorption capacity of each IL@polymer decreased with the increase of absorption temperature, which is attributed to the exothermic nature of adsorption. Thus, the interactive binding forces between adsorbate and adsorbent decrease. For instance, SO_2 capacity of $[N_{1111}][TTFA]$@polymer under 1 bar decreased from 7.51 mmol g^{-1} at 20°C to 5.98 mmol g^{-1} at 50°C, indicating that the loaded SO_2 can be released under high temperature. Additionally, SO_2 capture by raw material $[N_{1111}][OH]$@polymer at 20°C was also determined with the capacities of 0.67 and 10.39 mmol g^{-1} under 0.05 and 1 bar, respectively, due to the strong basicity of [OH] anions, which may result in difficult desorption.[53]

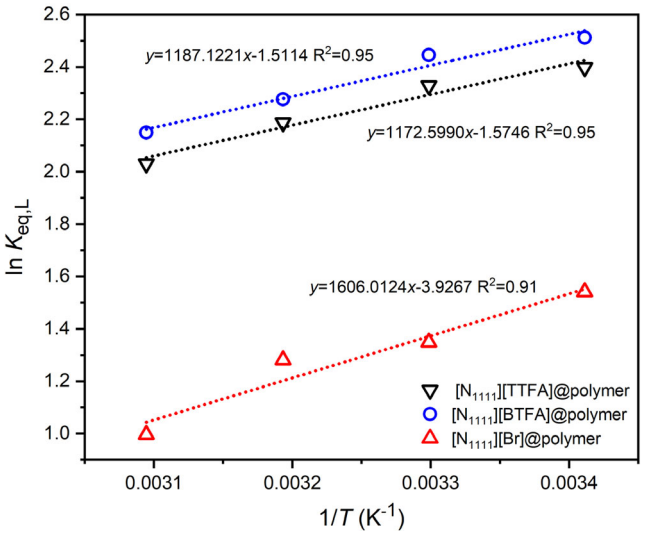

FIGURE 8 Linear correlation between ln $K_{eq,L}$ and $1/T$.

Adsorption isotherm models can provide mechanism information of the adsorption process, which is important for the design of adsorption system.[73,74] Here, the adsorption isotherms, formed from equilibrium adsorption capacity (q_e, in mmol g^{-1}) at different temperatures and partial pressures, on these IL@polymers were correlated using the Langmuir model, Freundlich model, and Sips model based on the following equations, respectively[75]:

$$q_e = \frac{q_{max} \times K_L \times P_e}{1 + K_L \times P_e}$$

$$q_e = K_F \times P_e^{N_F}$$

$$q_e = \frac{q_{max} \times K_S \times P_e^{N_S}}{1 + K_S \times P_e^{N_S}}$$

where q_{max} represents the maximum adsorption capacity in mmol g^{-1}, P_e denotes the equilibrium pressure in bar, K_L in bar^{-1} is the Langmuir constant, K_F in mmol g^{-1} bar^{-N_F} is the Freundlich constant, K_S in bar^{-N_S} is the Sips constant, N_F and N_S are dimensionless parameters that qualitatively characterize the heterogeneity of the adsorbate-

TABLE 3 The thermodynamic parameters, including standard enthalpy change ($\Delta H°$, in kJ mol^{-1}), standard entropy change ($\Delta S°$, in J mol^{-1} K^{-1}), and standard Gibbs free energy change ($\Delta G°$, in kJ mol^{-1}) under different temperatures (T, in°C) calculated from equilibrium constant ($K_{eq,L}$, dimensionless).

IL@polymer	$\Delta H°$	$\Delta S°$	R^2	$\Delta G°$ 20°C	30°C	40°C	50°C
$[N_{1111}][TTFA]$@polymer	−9.75	−13.09	0.946	−5.84	−5.87	−5.69	−5.45
$[N_{1111}][BTFA]$@polymer	−9.87	−12.57	0.953	−6.12	−6.16	−5.93	−5.77
$[N_{1111}][Br]$@polymer	−13.35	−32.65	0.911	−3.76	−3.40	−3.34	−2.68

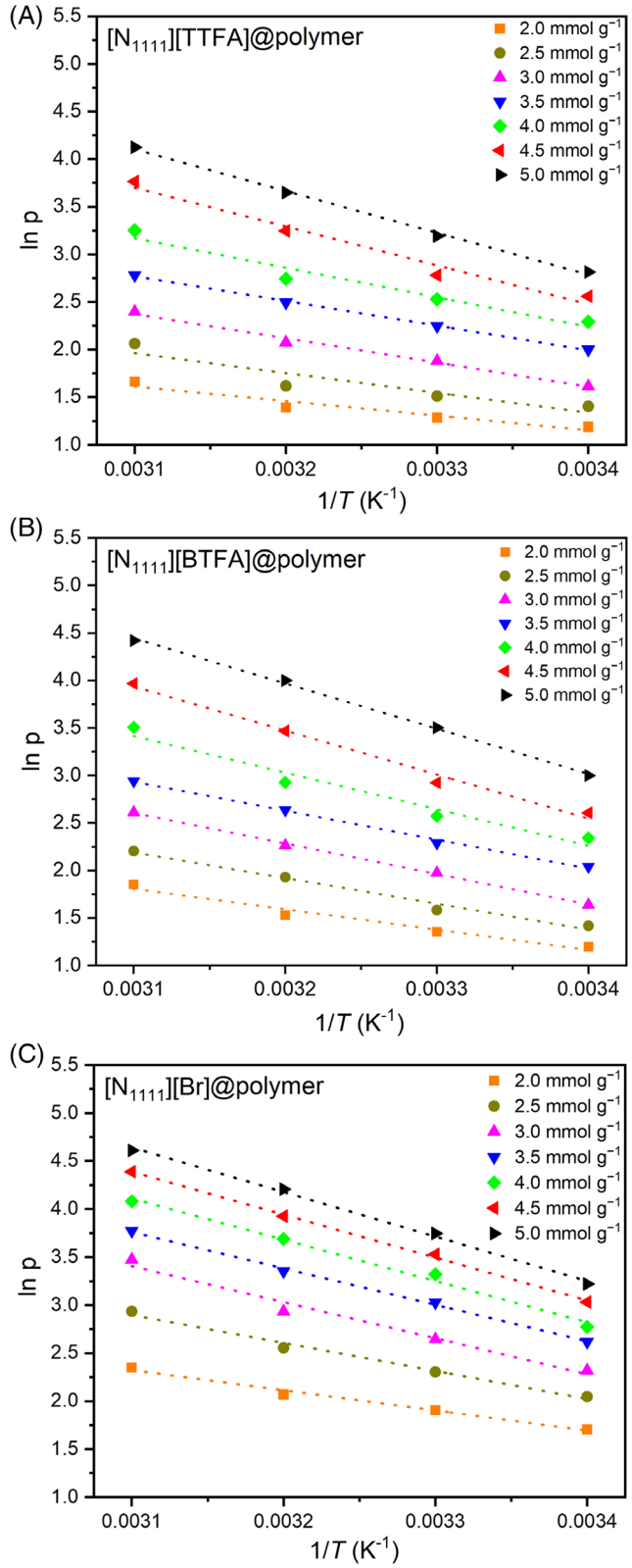

FIGURE 9 ln *p* versus 1/*T* for estimation of isosteric adsorption heats of SO_2 on $[N_{1111}][TTFA]$@polymer (A), $[N_{1111}][BTFA]$@polymer (B), and $[N_{1111}][Br]$@polymer (C).

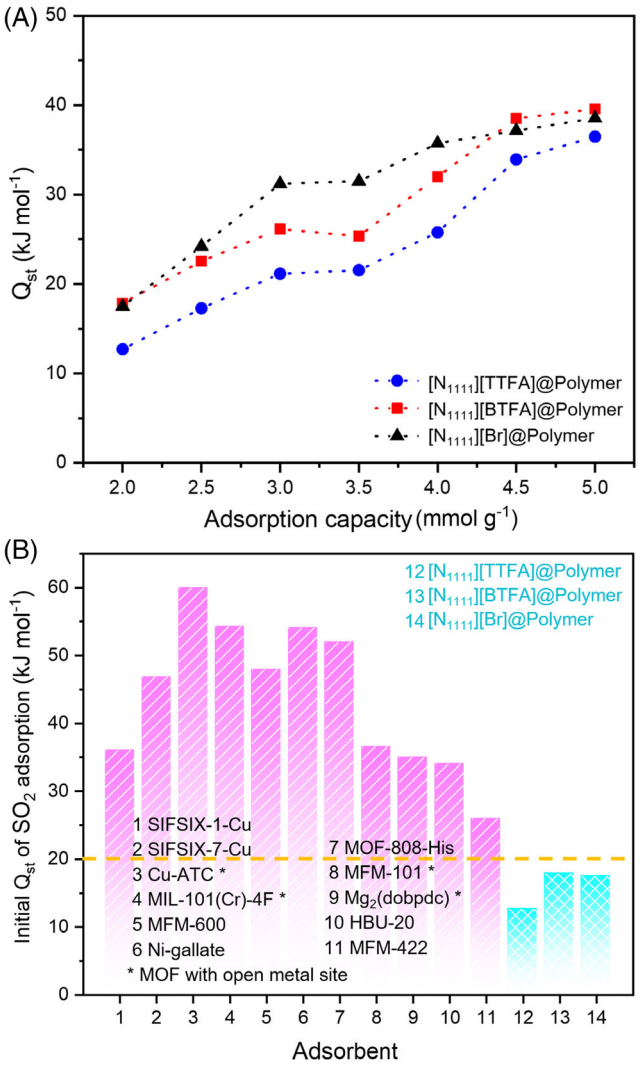

FIGURE 10 (A) The isosteric heat (Q_{st}) of SO_2 adsorption on the IL@polymers as a function of SO_2 loading; (B) The comparison of initial Q_{st} of SO_2 adsorption on these IL@polymers and typical other 11 reported adsorbents collected in Ref. [81]. Sorbents marked with * are related to MOFs with open metal sites.

adsorbent system. Compared to the single-parameter Langmuir and Freundlich models, the three-parameter Sips model is clearly the combination form of the aforementioned two models and is suitable for predicting the adsorption performance of heterogeneous systems at a wide range of pressures. The fitting results of these models are also illustrated in Figure 7 while the relevant parameters and correlation coefficients (R^2) are listed in Appendix S1. It can be seen that all fitting results were in agreement with the experimental data, and the Sips model shows the best fit with a high correlation coefficient ($R^2 > 0.99$) among these models. Additionally, the larger is N_S the more heterogeneous the system is. As the listed values of N_S are all greater than unity ($N_S > 1$), all SO_2 adsorptions on IL@polymers are heterogeneous.

3.3 | SO_2 adsorption thermodynamics

In order to better understand the adsorption mechanism, the thermodynamic parameters such as the standard enthalpy change (ΔH°, in kJ mol^{-1}), the standard Gibbs free energy change (ΔG°, in kJ mol^{-1}),

and the standard entropy change (ΔS°, in J mol^{-1} K^{-1}) were estimated by the following equations, using the equilibrium constant (K_{eq}, dimensionless):

$$\ln K_{eq} = \frac{\Delta S^\circ}{R} - \frac{\Delta H^\circ}{RT}$$

$$\Delta G^\circ = -RT \ln K_{eq}$$

Although the aforementioned models are suitable for calculating the thermodynamic parameters, the constants K_L, K_F, and K_S of the Langmuir, Freundlich, and Sips are dimensional, and it is necessary to convert those constants from dimensional (with a unit) to dimensionless (without unit) before applying them as the thermodynamic equilibrium constant for the calculation. It is reported that K_F is not suitable for calculation because its unit cannot be converted to dimensionless easily, and K_{eq} can be calculated from K_L and K_S according to the following equations,[76,77]

$$K_{eq,L} = K_L \times P^\circ$$

$$K_{eq,S} = \sqrt[N_S]{K_S} \times P^\circ$$

P° in bar is the standard pressure ($P^\circ = 1$ bar). The curves of ln $K_{eq,L}$ versus $1/T$ are plotted in Figure 8. Although there is better conformity of the adsorption process with the Sips model than with the Langmuir model, the estimated data (from the plots of ln $K_{eq,S}$ vs. $1/T$) proved to be unrealistic and hence unreliable and not considered in this work.[78] The obtained ΔH°, ΔS°, and R^2 based on $K_{eq,L}$ as well as ΔG° are listed in Table 3. The negative values of ΔG° indicated the favorable SO_2 adsorptions in each IL@polymer adsorbent under the experimental conditions, while the negative values of ΔH° indicated the exothermic adsorption process and the physical interaction between SO_2 and each IL@polymer adsorbent. In addition, the negative ΔS° values indicated that the degree of disorder of the system becomes smaller due to the interactions. The spontaneity of the adsorption process is governed by the ΔG, following the equation $\Delta G^\circ = \Delta H^\circ - T\Delta S^\circ$. Here, $\Delta H^\circ < 0$ and $\Delta S^\circ < 0$, but the value of $|\Delta H^\circ|$ was calculated and found to be higher than the value of $|T\Delta S^\circ|$. Thus, the value of $\Delta H^\circ - T\Delta S^\circ$ is always negative, indicating that the adsorption processes were spontaneous. Take [N_{1111}][TTFA]@polymer as an example; the values of ΔH° and ΔS° were calculated to be -9.75 kJ mol^{-1} and -13.09 J mol^{-1} K^{-1}, respectively, resulting in the values of $\Delta H^\circ - T\Delta S^\circ$ in the range of -5.9 to -5.5 kJ mol^{-1}. Therefore, the sign of ΔG° was determined by that of ΔH°. Thus, the SO_2 adsorption is an entropy-driven process.

As a key thermodynamic quantity in the adsorption process, the isosteric heat (Q_{st}, in kJ mol^{-1}) could be obtained from the SO_2 adsorption isotherms at 20, 30, 40, and 50°C using Clausius-Clapeyron equation:

$$\ln p = \frac{Q_{st}}{RT} + C$$

where p (in bar) is the pressure at a fixed adsorbed amount of SO_2 (2–5 mmol g^{-1} with an interval of 0.5 mmol g^{-1}), T is the adsorption temperature in K, R is the gas constant with the value of 8.314 J mol^{-1} K^{-1}, and C is a constant. The fitting plots of ln p against $1/T$ (in 1 K^{-1}) were depicted in Figure 9 with good straight lines at the aforementioned adsorbed quantities for each IL@polymer, and Q_{st} could be obtained from the slope. The relationship between isosteric heat of SO_2 adsorptions on the IL@polymers and the adsorbed amount of SO_2 was illustrated in Figure 10A. The results showed that the values of initial Q_{st} of these IL@polymers are slightly lower than 20 kJ mol^{-1}, but higher than the values of ΔH°, possibly because of the host–guest interactions.[79] The low values of Q_{st} suggested that the adsorption processes are weak chemical and SO_2 could be desorbed relatively easily from the adsorption sites as well as the sorbents could be regenerated energy-savingly.[80] Moreover, the Q_{st} of these IL@polymers is lower than other reported adsorbents, such as metal–organic frameworks (MOFs),[81–83] which the Q_{st} values are usually higher than 20 kJ mol^{-1} (Figure 10B). The results are consistent with the large pores of IL@polymers, reducing the strength of host-guest interactions.[84] Interestingly, the value of Q_{st} gradually increases with the increase of SO_2 loading, suggesting the surface uniformity of these IL@polymers and the partial structural changes of the network during SO_2 loading.[85]

3.4 | Adsorption–desorption SO_2 cycles

It is known that the cycle stability plays an essential role in adsorbents' practical applications. In order to evaluate the reversibility of these IL@polymers, cycles of adsorption–desorption of SO_2 were performed. The adsorptions were tested at 20°C and 0.05 bar SO_2, and desorptions were performed at 80°C and 1 bar N_2, and the results were illustrated in Figure 11. It shows that the capacities of SO_2 adsorption on conjugated carbanion-derived IL@polymers were all around 3 mmol g^{-1}, indicating that these functional IL@polymers

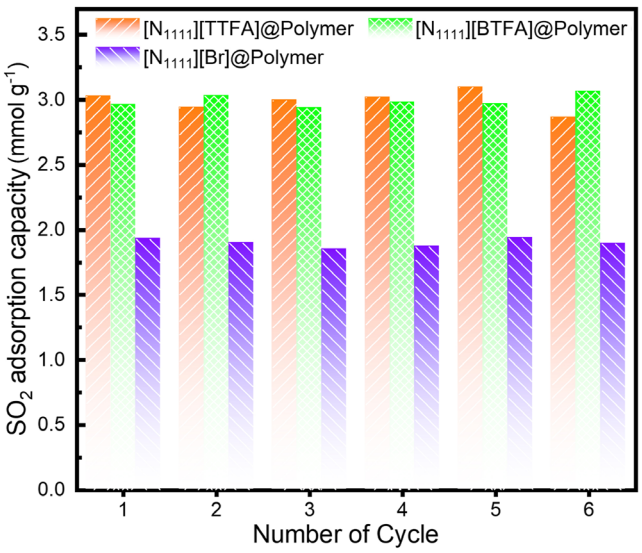

FIGURE 11 Cycles of adsorptions at 20°C and 0.05 bar SO_2 and desorptions at 80°C and 1 bar N_2.

could be highly recycled with the SO_2 adsorption capacity remaining steady. Thus, the SO_2 adsorptions by these IL@polymers are highly reversible.

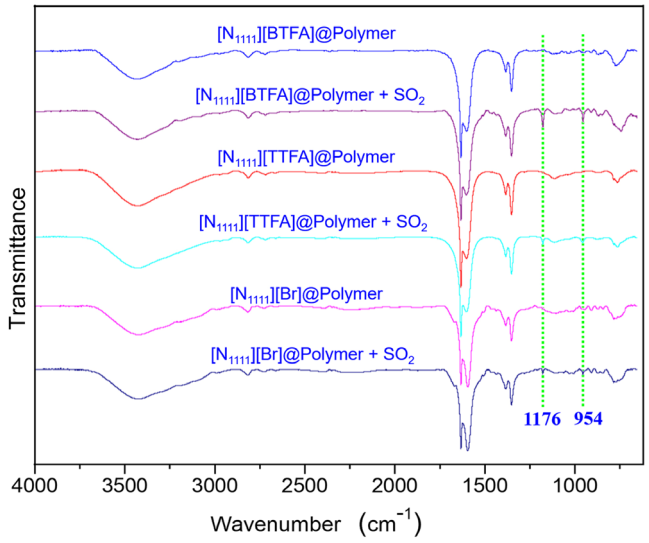

FIGURE 12 FT-IR spectra of $[N_{1111}][BTFA]$@polymer, $[N_{1111}][TTFA]$@polymer, and $[N_{1111}][Br]$@polymer before and after the adsorption of SO_2 at 20°C and 1 bar.

3.5 | SO_2 adsorption mechanism

As aforementioned before, the average pore sizes of these IL@polymers were higher than 50 nm and their BET surface areas were lower than 25 $m^2\ g^{-1}$. Therefore, all these sorbents were found to be macroporous materials with low BET surface areas. Thus, it is crucial to investigate the mechanism of SO_2 adsorption on these IL@polymers. Here, SEM and mapping, FT-IR, and quantum chemical calculations were used as typical methods to study the SO_2 adsorption mechanism.

The SEM and mapping images after SO_2 adsorption in these IL@polymers were also measured (Figure S1). Compared with the morphologies of neat IL@polymers, that of IL@polymers after SO_2 capture seemed to show no significant change. Besides, the mapping of these samples indicated that SO_2 molecules were uniformly adsorbed on the surface of the IL@polymers. In addition, the adsorption mechanism was analyzed by FT-IR spectra. Figure 12 shows the FT-IR spectra of these IL@polymer sorbents before and after the adsorption. Clearly, compared with the spectra of SO_2-free IL@polymer samples, two peaks at 1176 and 954 cm^{-1} appeared as a result of SO_2 adsorption, which could be assigned to the vibrations of S═O and S—O bonds, respectively.[54,71] According to the literatures,[86,87] these typical peaks indicated the charge-transfer

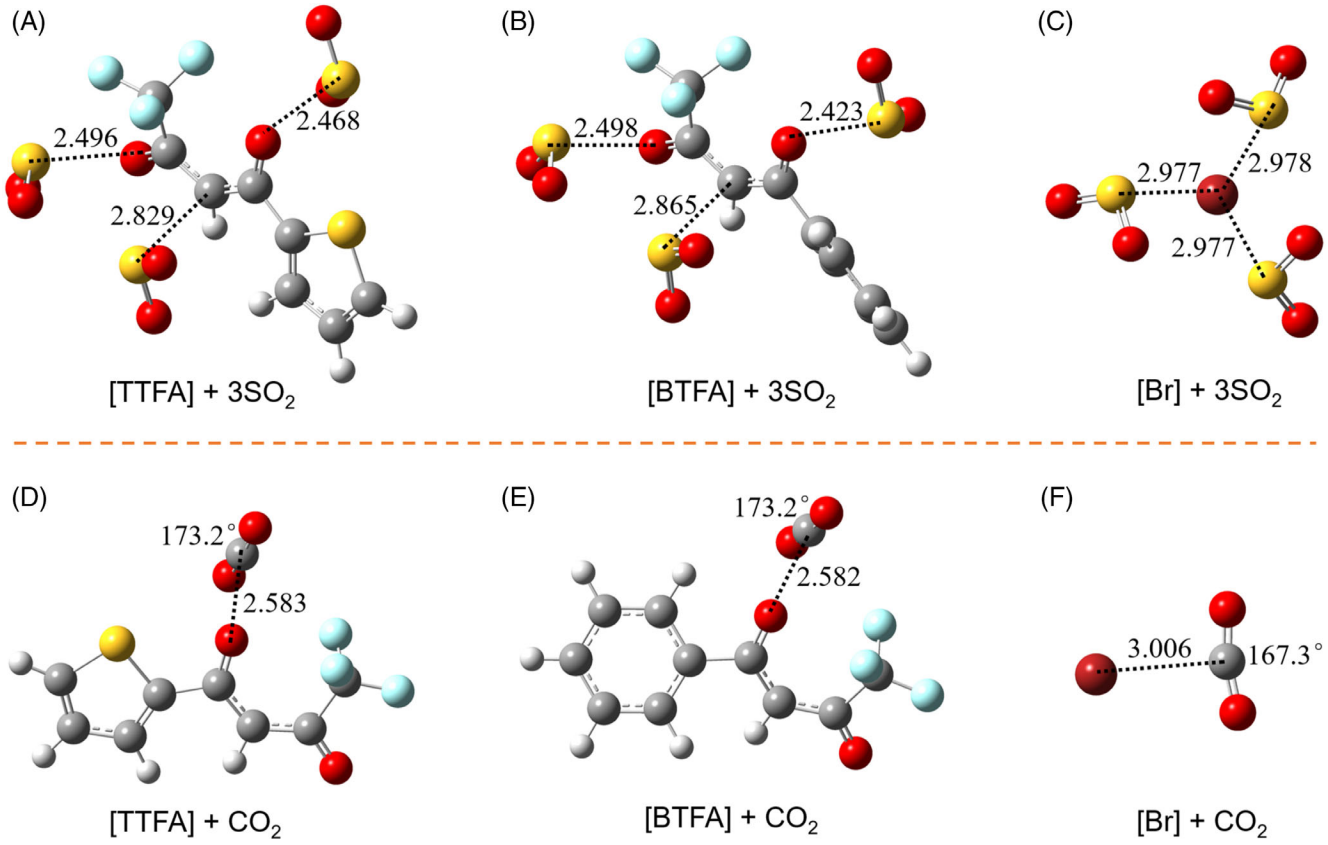

FIGURE 13 Optimized structures based on the anions and SO_2 or CO_2. (A), $[TTFA] + 3SO_2$; (B) $[BTFA] + 3SO_2$; (C) $[Br] + 3SO_2$; (D) $[TTFA] + CO_2$; (E) $[BTFA] + CO_2$; (F) $[Br] + CO_2$. Note that the van der Waals radii of atoms are 1.70 Å for C (gray), 1.20 Å for H (white), 1.52 Å for O (red), 1.80 Å for S (yellow), 1.47 Å for F (green), and 1.85 Å for Br (dark red), respectively.[92]

quasi-chemisorption of SO_2 between IL@polymers and SO_2. That is consistent with the results of isosteric heat analysis (Q_{st} < 20 kJ mol^{-1}), which leads to the quasi-chemical interaction of anions with SO_2. Thus, the charge-transfer interaction between active sites on IL@polymer and SO_2 may attribute to a kind of quasi-chemisorption of SO_2.[2] Furthermore, dispersion-corrected density functional theory (DFT-D3(BJ)) calculation at the B3LYP/6-31++G (p,d) level[88–90] using the Gaussian 16 program[91] was used to study the interactions between SO_2 and anions ([TTFA], [BTFA], and [Br]), and the optimized structures of [TTFA] + $3SO_2$, [BTFA] + $3SO_2$, and [Br] + $3SO_2$ are illustrated in Figure 13A–C. Clearly, all the distances between the S atom in SO_2 and the active atom in anions were predicted to be shorter than the sum of the radii of two atoms (18%–28%), suggesting that all these anions could interact with three SO_2 molecules. These results are consistent with the results of Q_{st} calculation, which suggest the weak chemical interactions between adsorbate and adsorbents.

3.6 | SO_2/CO_2 selectivity

The performances of CO_2 capture at 20°C under different partial pressures were also determined to test the SO_2/CO_2 selectivity (Figure 13A–C). It is illustrated that the SO_2 uptake of each adsorbent at 20°C under high pressure (1 bar) was higher than 7 mmol g^{-1}, while the CO_2 isotherm on each adsorbent was obviously flatter and displayed only 0.1–0.4 mmol g^{-1} even at 20°C and 1 bar. Additionally, CO_2 capacities of conjugated carbanion-derived IL@polymers (0.12 mmol g^{-1} on $[N_{1111}]$[TTFA]@polymer and 0.15 mmol g^{-1} on $[N_{1111}]$[BTFA]@polymer) were much lower than that of bromide-based $[N_{1111}]$[Br]@polymer (0.34 mmol g^{-1}), probably due to the dispersed negative charges on conjugated carbanion anions while the concentrated negative charge on bromide anion resulted in the weakened carbanion-CO_2 interaction. Besides, the calculated ∠O═C═O angles in the optimized structures of [TTFA] + CO_2, [BTFA] + CO_2, and [Br] + CO_2 amount to 173.2°, 173.2°, and 167.3°, respectively,

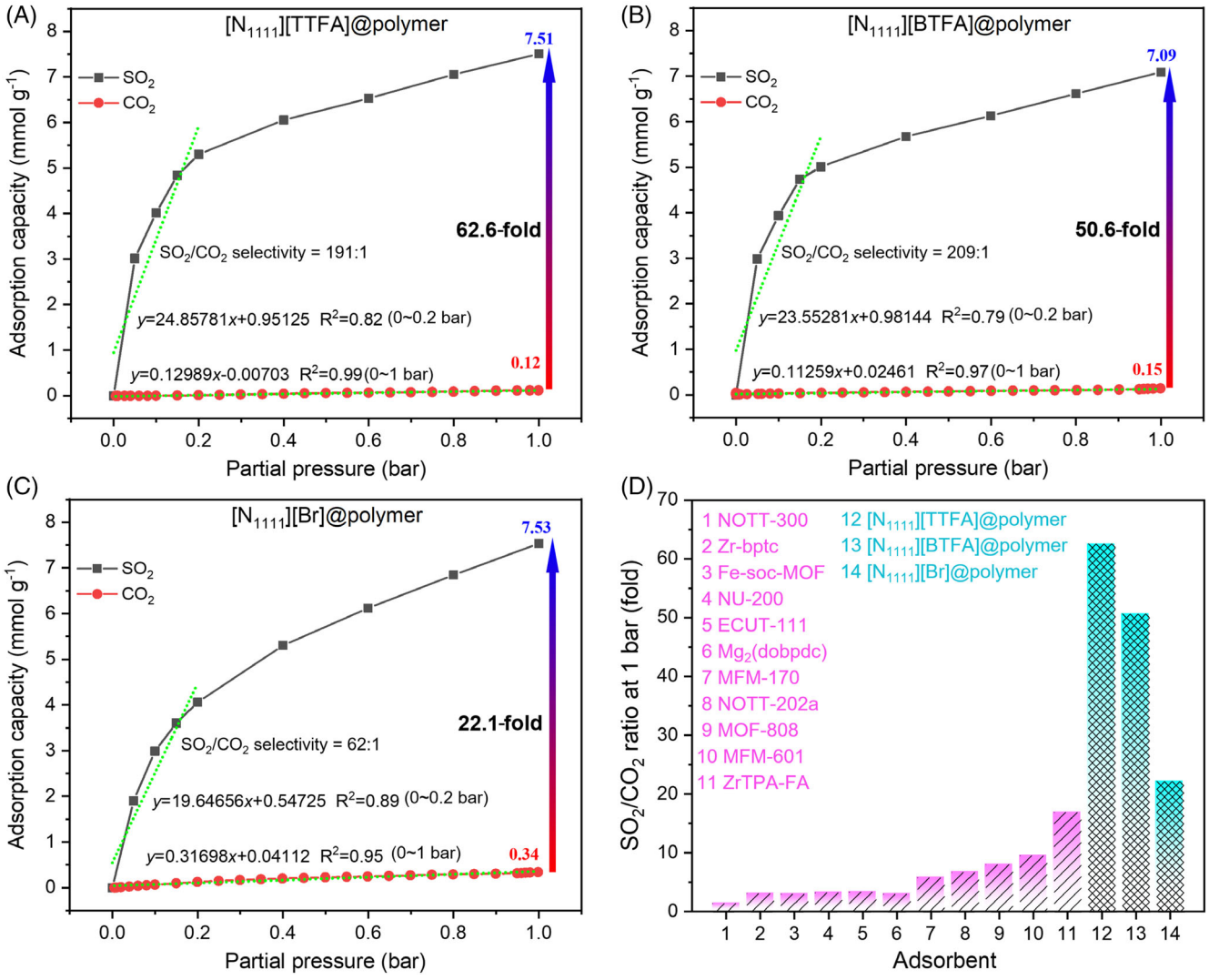

FIGURE 14 Adsorption curves of SO_2 and CO_2 by $[N_{1111}]$[TTFA]@polymer (A), $[N_{1111}]$[BTFA]@polymer (B), and $[N_{1111}]$[Br]@polymer (C) at 20°C. (D) Comparison of the adsorption amount ratio of SO_2/CO_2 at 1 bar for IL@polymer sorbents (at 20°C) and typical reported MOFs collected in ref. [80] (at 25°C).

indicating that [Br] anion could interact with CO_2 more efficiently than [TTFA] and [BTFA] anions (Figure 13D–F). Thereby, the adsorption amount ratios of SO_2/CO_2 at 20°C and 1 bar were calculated to be 62.6-fold, 50.6-fold, and 22.1-fold for $[N_{1111}]$[TTFA]@polymer, $[N_{1111}]$[BTFA]@polymer, and $[N_{1111}]$[Br]@polymer, respectively. Here, the "fold" could be used to describe the selectivity of SO_2 over CO_2, according to Farha et al's work.[80] Compared with most MOFs, these conjugated carbanion-derived IL@polymer sorbents exhibited more efficiency for SO_2/CO_2 separation (Figure 14D).

To evaluate the gas-selective separation performance of IL@polymer adsorbents, Henry's theory was used to calculate SO_2/CO_2 selectivity.[93] As shown in Figure 14A–C, the adsorption behavior of both SO_2 and CO_2 gas nearly obeys Henry's law in the low-pressure range (p < 0.2 bar), and the calculated Henry's law selectivity for SO_2/CO_2 at 20°C for $[N_{1111}]$[TTFA]@polymer, $[N_{1111}]$[BTFA]@polymer, and $[N_{1111}]$[Br]@polymer was 191, 209, and 62, respectively. Clearly, the SO_2/CO_2 Henry's law selectivities for conjugated carbanion-derived $[N_{1111}]$[TTFA]@polymer and $[N_{1111}]$[BTFA]@polymer were both more than three times that for bromide anion-derived $[N_{1111}]$[Br]@polymer, indicating the highly efficient selective SO_2 capture by conjugated carbanion-derived IL@polymer adsorbents.

3.7 | Effect of water on SO_2 adsorption

Due to the different hydrophobicity of these IL@polymer adsorbents, the performances of water adsorption were also studied, and the results are illustrated in Figure 15. Weight capacities (in g g^{-1}) and molar capacities (in mmol g^{-1}) were both calculated. For industry application, the weight capacities of SO_2 (0.05 bar) were measured to be 0.19, 0.19, and 0.12 g $g,^{-1}$ while that of water were measured to be 0.15, 0.17, and 0.27 g g^{-1} for $[N_{1111}]$[TTFA]@polymer, $[N_{1111}]$[BTFA]@polymer, and $[N_{1111}]$[Br]@polymer, respectively. Thus, the ratios of SO_2/H_2O were calculated to be 1.27, 1.12, and 0.44. Clearly, the results indicated that the bromide anion-derived $[N_{1111}]$[Br]@polymer adsorbent is more efficient for the adsorption of water than SO_2, while the conjugated carbanion-derived $[N_{1111}]$[TTFA]@polymer and $[N_{1111}]$[BTFA]@polymer adsorbents are highly efficient for the adsorption of SO_2 than water. Additionally, the difference in capture capacity between SO_2 and water for $[N_{1111}]$[TTFA]@polymer adsorbent is larger than that for $[N_{1111}]$[BTFA]@polymer, exhibiting obvious advantages in SO_2/H_2O selective adsorption by tunable conjugated carbanion-derived IL@polymers. It is known that the molar mass of H_2O (18 g mol^{-1}) is much smaller than that of SO_2 (64 g mol^{-1}), meaning water contains 3.5 times as many molecules as SO_2 for the same mass. Here, the molar capacities of SO_2 were calculated to be 3.02, 2.99, and 1.92 mmol g^{-1}, while that of water were calculated to be 8.49, 9.59, and 14.82 mmol g^{-1} for $[N_{1111}]$[TTFA]@polymer, $[N_{1111}]$[BTFA]@polymer, and $[N_{1111}]$[Br]@polymer, respectively. Thus, the ratios of SO_2/H_2O were calculated to be 0.36, 0.31, and 0.13, also suggesting that conjugated carbanion-derived adsorbents are highly efficient for the selective adsorption of SO_2. Therefore, through adjusting the structure of anions of PILs, the hydrophobicity of these IL@polymer adsorbents could be tuned, and the efficient selective adsorption of SO_2 could be obtained by functional IL-based materials.

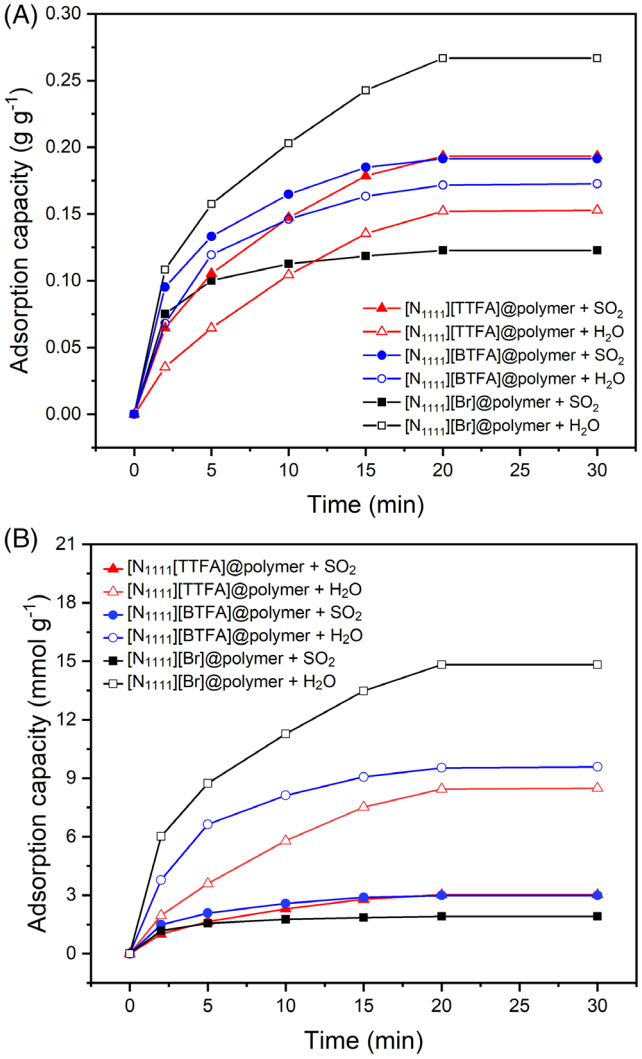

FIGURE 15 Capture of 5 vol% SO_2 or water at 20°C and 1 bar by IL@polymers in g g^{-1} (A) and mmol g^{-1} (B).

4 | CONCLUSION

In summary, two kinds of novel conjugated carbanion anion-derived IL-based porous polymers were developed for selective SO_2 capture. Surface morphology, porosity, contact angle, and stability were systematically investigated, exhibiting the macroreticular internal structures and the macropores (>50 nm) as well as an enhanced hydrophobicity. The effect of SO_2 partial pressure and temperature on SO_2 adsorption capacity by IL-derived polymers was investigated, and the Sips model is suitable for predicting adsorption performance. Compared with bromide-based IL@polymer, an enhanced hydrophobicity as well as the efficient capacity of SO_2 (>7 mmol g^{-1}) and high selectivity of SO_2/CO_2 (62.6-fold) and SO_2/H_2O were obtained by conjugated carbanion-derived $[N_{1111}]$[BTFA]@polymer and $[N_{1111}]$

[TTFA]@polymers through carbanion-SO_2 interaction. Moreover, the calculated values of the initial isosteric heat of adsorption were in the range of 10–20 kJ mol^{-1} and increased with the increase of SO_2 loading. Thus, through heating or bubbling N_2 through IL@polymer sorbents, the captured SO_2 was easy to desorb and the IL-derived polymers could be recyclable. Besides, the results of FT-IR investigations suggested the SO_2··· IL@polymer charge-transfer quasi-chemical interaction. This method using conjugated carbanion functional groups opens a door to obtain enhanced hydrophobicity, SO_2 capture capacity as well as excellent SO_2/CO_2 selectivity and SO_2/H_2O selectivity by IL-based iPOMs.

AUTHOR CONTRIBUTIONS

Guokai Cui: Supervision, Conceptualization, Project administration, Funding acquisition, Resources, Investigation, Writing – original draft, Writing – review & editing. Yinfeng Chen: Investigation, Data curation, Visualization. Limin Xu: Formal analysis, Validation. Ruina Zhang: Methodology, Data curation, Visualization. Xu Wang: Formal analysis. Ying Zhou: Formal analysis, Funding acquisition. Quanli Ke: Formal analysis, Funding acquisition. Xiaopo Niu: Formal analysis. Xiangping Zhang: Resources, Formal analysis. Mingcai Teng: Formal analysis, Funding acquisition. Meichao Li: Formal analysis. Hanfeng Lu: Conceptualization, Project administration, Resources, Funding acquisition.

ACKNOWLEDGMENTS

This work was financially supported by the Key Research and Development Projects in Zhejiang Province (nos. 2024C03108, 2023C03127, 2024C03114, 2024C03121), the National Natural Science Foundation of China (no. 22378353, 22208300), the Zhejiang Provincial Natural Science Foundation of China (no. LTGS24E080008), and the Zhejiang Provincial Postdoctoral Science Foundation (no. ZJ2023145).

CONFLICT OF INTEREST STATEMENT

The authors have no conflict of competing interests.

DATA AVAILABILITY STATEMENT

The authors declare that the data that supports the findings of this study are available as a .pdf file and a .zip file in Supporting Information of this article. Specifically, the SEM images and EDS mapping images in Figure 3 and Figure S1, the full survey XPS spectra in Figure 4, the N_2 adsorption–desorption isotherms and pore sizes in Figure 5, the thermogravimetric analysis curves and water contact angles in Figure 6, and the FT-IR spectra in Figure 12 are available in the .zip file in Appendix S2. The analysis of commercialization performance, Figure S1 and the numerical data for Figures 7–11, 14 and 15 are provided in the .pdf file in Appendix S1, and the uncertainty associated with the measured experimental data was calculated to be ±0.07.

ORCID

Guokai Cui https://orcid.org/0000-0002-7223-2869
Xiangping Zhang https://orcid.org/0000-0002-1431-0873
Hanfeng Lu https://orcid.org/0000-0001-8934-8270

REFERENCES

1. Hanif MA, Ibrahim N, Abdul JA. Sulfur dioxide removal: An overview of regenerative flue gas desulfurization and factors affecting desulfurization capacity and sorbent regeneration. *Environ Sci Pollut Res*. 2020;27(22):27515-27540.
2. Zhang R, Tang L, Ge C, et al. Functional ionic liquids for SO_2 capture and conversion. *New J Chem*. 2025;49(23):9552-9571.
3. Zhang R, Ke Q, Zhang Z, Zhou B, Cui G, Lu H. Tuning functionalized ionic liquids for CO_2 capture. *Int J Mol Sci*. 2022;23(19):11401.
4. Suo X, Fu Y, Do-Thanh C-L, et al. CO_2 chemisorption behavior in conjugated carbanion-derived ionic liquids via carboxylic acid formation. *J Am Chem Soc*. 2022;144(47):21658-21663.
5. Huang Y, Cui G, Zhao Y, et al. Preorganization and cooperation for highly efficient and reversible capture of low-concentration CO_2 by ionic liquids. *Angew Chem Int Ed*. 2017;56(43):13293-13297.
6. Wang K, Zhang Z, Wang S, Jiang L, Li H, Wang C. Dual-tuning azole-based ionic liquids for reversible CO_2 capture from ambient air. *ChemSusChem*. 2024;17(16):e202301951.
7. Yoon B, Chen S, Voth GA. On the key influence of amino acid ionic liquid anions on CO_2 capture. *J Am Chem Soc*. 2024;146(2):1612-1618.
8. Liu Y, Dai Z, Zhang Z, et al. Ionic liquids/deep eutectic solvents for CO_2 capture: reviewing and evaluating. *Green Energy Environ*. 2021;6(3):314-328.
9. Chen B, Shu H, Guo Y, Xu Y. CO_2 capture and viscosity of metal chelate-based ionic liquids: influence of the structure and substitution of the azole-based anion. *J Mol Liq*. 2025;417:126574.
10. Cui G, Cheng Y, Zhang W, et al. Highly efficient CO_2 capture from open air and dilute gas streams by tunable azolate ionic liquids based deep eutectic solvents. *Chem Eng J*. 2025;505:159193.
11. Jiang L, Mei K, Chen K, Dao R, Li H, Wang C. Design and prediction for highly efficient SO_2 capture from flue gas by imidazolium ionic liquids. *Green Energy Environ*. 2022;7(1):130-136.
12. Ren S, Hou Y, Zhang K, Wu W. Ionic liquids: functionalization and absorption of SO_2. *Green Energy Environ*. 2018;3(3):179-190.
13. Cui G, Liu J, Lyu S, et al. SO_2 absorption in highly efficient chemical solvent AChBr + Gly compared with physical solvent ChBr + Gly. *J Mol Liq*. 2021;330:115650.
14. Cui G, Lin W, Ding F, et al. Highly efficient SO_2 capture by phenyl-containing azole-based ionic liquids through multiple-site interactions. *Green Chem*. 2014;16(3):1211-1216.
15. Zhou Z, Zhang P, Chang Y, Chen X. Highly efficient capture and removal of H_2S by multi-amine functionalized ionic liquids. *J Mol Liq*. 2023;392:123501.
16. Zhang X, Xiong W, Peng L, Wu Y, Hu X. Highly selective absorption separation of H_2S and CO_2 from CH_4 by novel azole-based protic ionic liquids. *AIChE J*. 2020;66(6):e16936.
17. Huang K, Wu Y-T, Hu X-B. Effect of alkalinity on absorption capacity and selectivity of SO_2 and H_2S over CO_2: substituted benzoate-based ionic liquids as the study platform. *Chem Eng J*. 2016;297:265-276.
18. Peng L, Shi M, Zhang X, et al. Facilitated transport separation of CO_2 and H_2S by supported liquid membrane based on task-specific protic ionic liquids. *Green Chem Eng*. 2022;3(3):259-266.
19. Zhai R, He X, Mei K, et al. Ultrahigh nitric oxide capture by tetrakis(azolyl)borate ionic liquid through multiple-sites uniform interaction. *ACS Sustain Chem Eng*. 2021;9(8):3357-3362.
20. Chen K, Shi G, Zhou X, Li H, Wang C. Highly efficient nitric oxide capture by azole-based ionic liquids through multiple-site absorption. *Angew Chem Int Ed*. 2016;55(46):14364-14368.
21. Sun Y, Gao M, Ren S, Zhang Q, Hou Y, Wu W. Highly efficient absorption of NO by amine-based functional deep eutectic solvents. *Energy Fuel*. 2020;34(1):690-697.
22. Liu J, Xu Y. NOx absorption and conversion by ionic liquids. *J Hazard Mater*. 2021;409:124503.

23. Li K, Zong K, Wang X, Cui G, Deng D. Ionic liquids and deep eutectic solvents for NH3 absorption and separation: a review. *New J Chem*. 2023;47(46):21426-21445.
24. Cai Z, Zhang J, Ma Y, et al. Chelation-activated multiple-site reversible chemical absorption of ammonia in ionic liquids. *AIChE J*. 2022;68(5):e17632.
25. Qiu R, Luo X, Yang L, et al. Regulated threshold pressure of reversibly sigmoidal NH_3 absorption isotherm with ionic liquids. *ACS Sustain Chem Eng*. 2020;8(3):1637-1643.
26. Tu W, Zeng S, Bai Y, Zhang X, Dong H, Zhang X. Theoretical insights into NH_3 absorption mechanisms with imidazolium-based protic ionic liquids. *Ind Chem Mater*. 2023;1(2):262-270.
27. Li K, Zhu Y, Shi S, et al. Machine learning models coupled with ionic fragment σ-profiles to predict ammonia solubility in ionic liquids. *Green Chem Eng*. 2025;6(2):223-232.
28. Peng L, Shi M, Pan Y, et al. Ultrahigh carbon monoxide capture by novel protic cuprous-functionalized dicationic ionic liquids through complexation interactions. *Chem Eng J*. 2023;451:138519.
29. Tao D-J, Chen F-F, Tian Z-Q, et al. Highly efficient carbon monoxide capture by carbanion-functionalized ionic liquids through C-site interactions. *Angew Chem Int Ed*. 2017;56(24):6843-6847.
30. Cui G, Jiang K, Liu H, et al. Highly efficient CO removal by active cuprous-based ternary deep eutectic solvents [HDEEA][Cl] + CuCl + EG. *Sep Purif Technol*. 2021;274:118985.
31. Kaur G, Kumar H, Singla M. Diverse applications of ionic liquids: A comprehensive review. *J Mol Liq*. 2022;351:118556.
32. Wang Y, He H, Wang C, et al. Insights into ionic liquids: from Z-bonds to quasi-liquids. *JACS Au*. 2022;2(3):543-561.
33. Lei Z, Chen B, Koo Y-M, MacFarlane DR. Introduction: ionic liquids. *Chem Rev*. 2017;117(10):6633-6635.
34. Wu W, Han B, Gao H, Liu Z, Jiang T, Huang J. Desulfurization of flue gas: SO_2 absorption by an ionic liquid. *Angew Chem Int Ed*. 2004;43(18):2415-2417.
35. Wang C, Cui G, Luo X, Xu Y, Li H, Dai S. Highly efficient and reversible SO_2 capture by tunable azole-based ionic liquids through multiple-site chemical absorption. *J Am Chem Soc*. 2011;133:11916-11919.
36. Wang L, Zhang Y, Liu Y, Xie H, Xu Y, Wei J. SO_2 absorption in pure ionic liquids: solubility and functionalization. *J Hazard Mater*. 2020;392:122504.
37. Cui G, Lyu S, Wang H, Li Z, Zhang R, Wang J. Tuning the structure of pyridinolate-based functional ionic liquids for highly efficient SO_2 absorption. *Fuel*. 2021;303:121311.
38. Xia L, Cui Q, Suo X, et al. Efficient, selective, and reversible SO_2 capture with highly crosslinked ionic microgels via a selective swelling mechanism. *Adv Funct Mater*. 2018;28(13):1704292.
39. Li X, Chen K, Guo R, Wei Z. Ionic liquids functionalized MOFs for adsorption. *Chem Rev*. 2023;123(16):10432-10467.
40. Valencia-Loza SJ, López-Olvera A, Martínez-Ahumada E, et al. SO_2 capture and oxidation in a Pd6L8 metal–organic cage. *ACS Appl Mater Interfaces*. 2021;13(16):18658-18665.
41. Zhang R, Zhang Z, Ke Q, Zhou B, Cui G, Lu H. Covalent organic frameworks with ionic liquid-moieties (ILCOFs): structures, synthesis, and CO2 conversion. *Nanomaterials*. 2022;12(20):3615.
42. Zhu H, Lin W, Li Q, et al. Bipyridinium-based ionic covalent triazine frameworks for CO_2, SO_2, and NO capture. *ACS Appl Mater Interfaces*. 2020;12(7):8614-8621.
43. Zhang R, Cui G, Wang X, et al. Ionic liquid-based advanced porous organic hyper-crosslinked polymers (ILHCPs) for CO_2 capture and conversion. *Chem Eng J*. 2024;489:151102.
44. Nie X, Qiu X, Zhang R, et al. Tunable and functional ionic liquids embedded hyper-Crosslinked polymers as robust H_2O-tolerant adsorbents for highly efficient gaseous toluene capture. *Chem Eng J*. 2025;505:159467.
45. Tan LC, Calix EM, Rene ER, Nancharaiah YV, van Hullebusch ED, Lens PNL. Amberlite IRA-900 ion exchange resin for the sorption of selenate and sulfate: equilibrium, kinetic, and regeneration studies. *J Environ Eng*. 2018;144(11):4018110.
46. Abu A, Abdullah N. Sorption and thermodynamic study of nitrate removal by using Amberlite IRA 900 (AI900) resin. *Mater Today Proc*. 2021;41:102-108.
47. Gao S, Zhang P, Wang Z, Cui G, Qiu J, Wang J. Ionic liquid functionalized 3D mesoporous FDU-12 for effective SO_2 capture. *ACS Sustain Chem Eng*. 2020;8(1):586-593.
48. Han B, Liu W, Li J, et al. Catalytic hydrodechlorination of triclosan using a new class of anion-exchange-resin supported palladium catalysts. *Water Res*. 2017;120:199-210.
49. Kumar KV, Gadipelli S, Wood B, et al. Characterization of the adsorption site energies and heterogeneous surfaces of porous materials. *J Mater Chem A*. 2019;7(17):10104-10137.
50. Ng KC, Burhan M, Shahzad MW, Ismail AB. A universal isotherm model to capture adsorption uptake and energy distribution of porous heterogeneous surface. *Sci Rep*. 2017;7(1):10634.
51. Al-Ghouti MA, Da'ana DA. Guidelines for the use and interpretation of adsorption isotherm models: a review. *J Hazard Mater*. 2020;393:122383.
52. Cui G, Zhao N, Li Y, et al. Limited number of active sites strategy for improving SO_2 capture by ionic liquids with fluorinated acetylacetonate anion. *ACS Sustain Chem Eng*. 2017;5(9):7985-7992.
53. Liang C, Li H. Absorption of SO_2 by ionic liquid [BMIM]OH. *Chem Ind Eng*. 2019;36(4):18-22.
54. Cui G, Zheng J, Luo X, et al. Tuning anion-functionalized ionic liquids for improved SO_2 capture. *Angew Chem Int Ed*. 2013;52(40):10620-10624.
55. Cui G, Zhang F, Zhou X, Li H, Wang J, Wang C. Tuning the basicity of cyano-containing ionic liquids to improve SO_2 capture through cyano–sulfur interaction. *Chem-Eur J*. 2015;21(14):5632-5639.
56. Zhang F, Cui G, Zhao N, Huang Y, Zhao Y, Wang J. Improving SO_2 capture by basic ionic liquids in an acid gas mixture (10% vol SO_2) through tethering a formyl group to the anions. *RSC Adv*. 2016;6(89):86082-86088.
57. Ding F, Zheng J, Chen Y, et al. Highly efficient and reversible SO_2 capture by surfactant-derived dual functionalized ionic liquids with metal chelate cations. *Ind Eng Chem Res*. 2014;53(48):18568-18574.
58. Wang C, Zheng J, Cui G, Luo X, Guo Y, Li H. Highly efficient SO_2 capture through tuning the interaction between anion-functionalized ionic liquids and SO_2. *Chem Commun*. 2013;49(12):1166-1168.
59. Hong SY, Im J, Palgunadi J, et al. Ether-functionalized ionic liquids as highly efficient SO_2 absorbents. *Energ Environ Sci*. 2011;4(5):1802-1806.
60. Wang J, Zeng S, Bai L, Gao H, Zhang X, Zhang S. Novel ether-functionalized pyridinium chloride ionic liquids for efficient SO_2 capture. *Ind Eng Chem Res*. 2014;53(43):16832-16839.
61. Yang D, Hou M, Ning H, et al. Reversible capture of SO_2 through functionalized ionic liquids. *ChemSusChem*. 2013;6(7):1191-1195.
62. Cui G, Zhang F, Zhou X, Huang Y, Xuan X, Wang J. Acylamido-based anion-functionalized ionic liquids for efficient SO_2 capture through multiple-site interactions. *ACS Sustain Chem Eng*. 2015;3(9):2264-2270.
63. Cui G, Lyu S, Zhang F, et al. Tuning ionic liquids with functional anions for SO_2 capture through simultaneous cooperation of N and O chemical active sites with SO_2. *Ind Eng Chem Res*. 2020;59(49):21522-21529.
64. Cui G, Li Y, Liu J, Wang H, Li Z, Wang J. Tuning environmentally friendly chelate-based ionic liquids for highly efficient and reversible SO_2 chemisorption. *ACS Sustain Chem Eng*. 2018;6(11):15292-15300.
65. Jiang L, Pan M, Wang S, et al. Tunable and facile preparation of chelate-based ionic liquids for highly efficient SO_2 separation under low concentration in flue gas. *Sep Purif Technol*. 2023;318:123979.

66. Wu L, An D, Dong J, Zhang Z, Li B-G, Zhu S. Preparation and SO_2 absorption/desorption properties of crosslinked poly(1,-1,3,3-tetramethylguanidine acrylate) porous particles. *Macromol Rapid Commun*. 2006;27(22):1949-1954.
67. An D, Wu L, Li B-G, Zhu S. Synthesis and SO_2 absorption/desorption properties of poly(1,1,3,3-tetramethylguanidine acrylate). *Macromolecules*. 2007;40(9):3388-3393.
68. An X-C, Li Z-M, Zhou Y, Zhu W, Tao D-J. Rapid capture and efficient removal of low-concentration SO_2 in simulated flue gas by hypercrosslinked hollow nanotube ionic polymers. *Chem Eng J*. 2020;394:124859.
69. Li L, da Silva I, Kolokolov DI, et al. Post-synthetic modulation of the charge distribution in a metal–organic framework for optimal binding of carbon dioxide and sulfur dioxide. *Chem Sci*. 2019;10(5):1472-1482.
70. Mao F-F, Zhou Y, Zhu W, Sang X-Y, Li Z-M, Tao D-J. Synthesis of guanidinium-based poly(ionic liquids) with nonporosity for highly efficient SO2 capture from flue gas. *Ind Eng Chem Res*. 2021;60(16):5984-5991.
71. Tao H, Shi G, Jiang L, Lin W, Li H, Wang C. Tuning the anion for ultrahigh and selective adsorption of low-concentration SO_2 by functionalized ionic porous organic polymers. *Sep Purif Technol*. 2024;333:125974.
72. Suo X, Yu Y, Qian S, Zhou L, Cui X, Xing H. Tailoring the pore size and chemistry of ionic ultramicroporous polymers for trace sulfur dioxide capture with high capacity and selectivity. *Angew Chem Int Ed*. 2021;60(13):6986-6991.
73. Wang J, Guo X. Adsorption isotherm models: classification, physical meaning, application and solving method. *Chemosphere*. 2020;258:127279.
74. Chen T, Da T, Ma Y. Reasonable calculation of the thermodynamic parameters from adsorption equilibrium constant. *J Mol Liq*. 2021;322:114980.
75. Gu J, Shao P, Luo L, et al. Microporous triazine-based ionic hypercrosslinked polymers for efficient and selective separation of $H_2S/CH_4/N_2$. *Sep Purif Technol*. 2022;285:120377.
76. Tran HN, Lima EC, Juang R-S, Bollinger J-C, Chao H-P. Thermodynamic parameters of liquid–phase adsorption process calculated from different equilibrium constants related to adsorption isotherms: a comparison study. *J Environ Chem Eng*. 2021;9(6):106674.
77. Lima EC, Hosseini-Bandegharaei A, Moreno-Piraján JC, Anastopoulos I. A critical review of the estimation of the thermodynamic parameters on adsorption equilibria. Wrong use of equilibrium constant in the Van't Hoof equation for calculation of thermodynamic parameters of adsorption. *J Mol Liq*. 2019;273:425-434.
78. Adelodun AA, Ngila JC, Kim D-G, Jo Y-M. Isotherm, thermodynamic and kinetic studies of selective CO_2 adsorption on chemically modified carbon surfaces. *Aerosol Air Qual Res*. 2016;16(12):3312-3329.
79. Krishna R. Evaluation of procedures for estimation of the isosteric heat of adsorption in microporous materials. *Chem Eng Sci*. 2015;123:191-196.
80. Gong W, Xie Y, Yamano A, et al. Modulator-dependent dynamics synergistically enabled record SO_2 uptake in Zr(IV) metal–organic frameworks based on pyrene-cored molecular quadripod ligand. *J Am Chem Soc*. 2023;145(49):26890-26899.
81. Ren J, Zeng W, Ying Y, Liu D, Yang Q. Discovery of anion-pillared metal–organic frameworks for efficient SO/CO separation via computational screening. *AIChE J*. 2024;70(5):e18351.
82. Xiong X-H, Wei Z-W, Wang W, Meng L-L, Su C-Y. Scalable and depurative zirconium metal–organic framework for deep flue-gas desulfurization and SO_2 recovery. *J Am Chem Soc*. 2023;145(26):14354-14364.
83. Zhu Z, Wu K, Liu X, et al. Dense open metal sites in a microporous metal–organic framework for deep desulfurization with record-high sulfur dioxide storage density. *AIChE J*. 2022;68(9):e17811.
84. Li J, Smith GL, Chen Y, et al. Structural and dynamic analysis of sulphur dioxide adsorption in a series of zirconium-based metal–organic frameworks. *Angew Chem Int Ed*. 2022;61(36):e202207259.
85. Li W, Li J, Duong TD, et al. Adsorption of sulfur dioxide in Cu(II)-carboxylate framework materials: the role of ligand functionalization and open metal sites. *J Am Chem Soc*. 2022;144(29):13196-13204.
86. Yang T, Wang Y, Huang Z, Liu F, Liao Q, Zhao T. Deep eutectic solvents composed of 1-methyl-3-ethylimidazole halides and pyridine derivatives for efficient absorption and conversion of SO_2 into cyclic sulfites under ambient conditions. *Sep Purif Technol*. 2025;361:131475.
87. Liu P, Cai K, Zhang X, Zhao T. Effective absorption of SO_2 by imidazole-based protic ionic liquids with multiple active sites: thermodynamic and mechanical studies. *AIChE J*. 2022;68(4):e17596.
88. Becke AD. Density-functional thermochemistry. III. The role of exact exchange. *J Chem Phys*. 1993;98(7):5648-5652.
89. Becke AD. Density-functional exchange-energy approximation with correct asymptotic behavior. *Phys Rev A*. 1988;38(6):3098-3100.
90. Lee C, Yang W, Parr RG. Development of the Colle-Salvetti correlation-energy formula into a functional of the electron density. *Phys Rev B*. 1988;37(2):785-789.
91. Frisch MJ, Trucks GW, Schlegel HB, et al. *Gaussian 16 (revision C.01)*. Gaussian, Inc; 2016.
92. van der Bondi A. Waals volumes and radii. *J Phys Chem*. 1964;68(3):441-451.
93. Gu J, Yuan Y, Zhao T, Liu F, Xu Y, Tao D-J. Ionic-containing hypercrosslinked polymer: a promising bifunctional material for CO_2 capture and conversion. *Sep Purif Technol*. 2022;301:121971.

SUPPORTING INFORMATION

Additional supporting information can be found online in the Supporting Information section at the end of this article.

How to cite this article: Cui G, Chen Y, Xu L, et al. Carbanion engineering for highly efficient selective SO_2 capture by ionic liquids based commercializable polymers. *AIChE J*. 2025;71(11):e70023. doi:10.1002/aic.70023